

Mass balance of glaciers in Bhaga basin, Western Himalaya: a geospatial and temperature-weighted AAR based model approach

V. Nagajothi¹, M. Geetha Priya^{2,*}, Parmanand Sharma³ and I. M. Bahuguna⁴

¹Centre for Incubation, Innovation, Research and Consultancy, Jyothy Institute of Technology, Tataguni, Bengaluru 560 082, India

²School of Electronics Engineering, Vellore Institute of Technology, Chennai 600 127, India

³ESSO-National Centre for Polar and Ocean Research (Ministry of Earth Sciences, Government of India), Goa 403 804, India

⁴Space Applications Centre, Indian Space Research Organization, Ahmedabad 380 015, India

Several recent studies carried out in the Himalayan region suggest enhanced receding rate of glaciers during the last two decades. Glacier health can be assessed by monitoring various glacier dynamics that includes mass balance, accumulation area ratio (AAR), equilibrium line altitude (ELA), etc. Here AAR, ELA and regressed mass balance for nine glaciers of the Bhaga basin, Western Himalaya during 2008–18 are presented using high resolution Sentinel 2 (10 m) and Landsat 7/8 (30 m) data with improved AAR and degree day/temperature index (DD/TI) model. Transient snow line (TSL) and AAR derived from the model were used in different regression equations to estimate the mass balance in both glacier and basin scale. *In situ* precipitation and temperature data obtained from the automatic weather station located at Keylong, Himachal Pradesh were used in this model based approach. Overall, the data reveal that most of the glaciers have experienced critical thinning and lost huge ice mass in the range –6.07 m.w.e. to –9.06 m.w.e.

Keywords: Accumulation area ratio, glaciers, mass balance, snow line, temperature index.

THE Indian Himalaya is estimated to have $25,041 \pm 1726$ sq. km of glaciated area^{1,2}, which is the largest amount of freshwater storage outside the polar region³. This large geographic extent, with complex and extreme topography along with variable climatic conditions, results in an inhomogeneous set of glacial recessions⁴. The Himalayan glaciers are the major freshwater source for the northern states of India during summer months⁵. Recent studies have shown that from the beginning of the 21st century, glaciers of the Himalaya are shrinking at a faster rate^{6–9}. Local temperature and precipitation play an important role in the amount and time of melt of a glacier⁹. The literature related to the study of Himalayan glaciers

suggests that their melting will accelerate in the near future^{10–12}. This constant mass loss of glaciers could lead to retreat in glacier area until a new equilibrium with climate is reached¹³. This will further reduce run-off from the glaciers leading to water scarcity at the end of the century¹⁴. In addition, increasing population of the locality also demands proper management of water resources. Hence, it is important to understand the glacier-stored water to maintain and manage water resources in the Himalayan region.

Mass balance is one of the important metrics to measure the growth or decline of water stored in a glacier¹⁵. The study on mass balance of a glacier in spatial and temporal scale can provide information on glacier behaviour towards climatology and hydrology¹¹. There are direct and indirect methods to measure glacier mass balance. The direct measurement (glaciology method) includes *in situ* specific mass balance measurements using stakes and snow pits. Considering the fact that glaciers of the Himalaya are situated in a harsh environment, direct method is challenging and difficult both in terms of logistics and accessibility. Whereas satellite remote sensing offers a potential mode for monitoring glaciers on a large scale¹⁶. Mass balance of glaciers on a large scale is analysed using indirect methods such as geodetic, area accumulation ratio (AAR) and gravimetric methods using satellite data^{17–19}. Among these methods, the geodetic method is frequently used to estimate region-wide long-term mass balance^{20–24}. However, the digital elevation model (DEM) used in the geodetic method provides mass balance in a temporal gap of 5 to 10 years^{13,25}. The inter-annual and seasonal variations in mass balance cannot be estimated using the geodetic method. The satellite-based gravitational method can be used to estimate mass balance of high glacierized regions with coarser spatial resolution (~400 km). Hence individual glacier mass balance cannot be obtained using the gravimetric method^{13,26,27}. An empirical relation-based approach between surface mass balance and AAR provides an option to calculate

*For correspondence. (e-mail: geetha.sri82@gmail.com)

Table 1. Mass balance data for various glaciers in the Indian Himalaya from 1974 to 2018 using different methods. Measurements by GRACE (Gravity Recovery and Climate Experiment) satellites are not reported due to varying estimates of glacier mass changes for the Himalaya⁸

Glacier	Year	Method	Mass balance reported (m.w.e.)	Reference
Gara	1974–75	Glaciological	0.55	46
	1977–81		-0.75	47
	1982–83		0.34	48
	1986–87		+0.034	19
	1987–88		-0.086	
	2000–11	Geodetic	-0.98 ± 0.26/year	7
		AAR	-0.81 ± 0.26/year	
	TI	-0.73 ± 0.24/year		
	1985–86	TI	0.7 ± 0.41 to -1.1 ± 0.41	49
	2013–14			
Gor Garang	1982–83	Glaciological	1.02	47
	1986–87		47	19
	1987–88		0.016	
Shaune Garang	1982–83		0.11	50
	1982–92		-0.42	51
Naradu	1983–84		-0.26	52
Kolahari			-0.29	
Gor Garang	1985–86,	TI	1.5 ± 0.6 to -1.6 ± 0.6	49
	2013–14			
Naradu	2000–11	Geodetic	-0.83 ± 0.28/year	7
		AAR	-0.63 ± 0.19/year	
		TI	-0.61 ± 0.23/year	
	1985–86	TI	-0.2 ± 0.44 to -0.8 ± 0.44	44
	2013–14			
	2000–03	Residual accumulation and ablation techniques	-0.40/year	53
Shaune Garang	2000–11	Geodetic	-0.99 ± 0.35/year	7
		AAR	-1.01 ± 0.30/year	
		TI	-1.09 ± 0.33/year	
	1985–86	TI	0.8 ± 0.54 to -0.9 ± 0.54/year	49
	2013–14			
Nineteen glaciers of Baspa basin	2001–02	AAR	-0.9 to -0.78/year	17
Baspa basin	2000–11	Geodetic	-0.49/year	44
		AAR	-0.36/year	
		TI	-0.43/year	
Chotta Shigiri	1955–99	Geodetic	-0.3/year	54
	2000–14		-0.6/year	
	2002–03	Glaciological	-1.42	37
	2015–16		-0.84	45
	2016–17		-0.28	
	2017–18		-0.4	
Hamtah	2000–01		-1.31	55
Chandra basin	1999–2011	Geodetic	-0.68 ± 0.15/year	21
	2000–12		-0.65 ± 0.04/year	22
	2003–08		-0.65 ± 0.4/year	23
Bara Shigiri	2016–17	Glaciological	-0.56	45
	2017–18		-0.82	
Twelve selected glaciers of Chandra basin	1999–2000	IAAR	-0.79 ± 0.34/year	15
	2008–09			
146 Glaciers in the Chandra basin	1984–2012		-0.61 ± 0.46/year	13
Waren and Bhut basin	2004–05	Geodetic	-0.19/year	35
	2005–06		-0.27/year	
	2006–07		-0.23/year	
Patsio	2000–13	Geodetic	-0.31/year	25
	2015–16	Glaciological	-0.68	45
	2016–17		-0.45	

(Contd)

Table 1. (Contd)

Glacier	Year	Method	Mass balance reported (m.w.e.)	Reference
Dokirani	2015–16		–0.26	
Chorabari	2003–04	Geodetic	–0.74/year	20
	2015–16		–0.72	45
Batal	2016–17		–0.42	
	2017–18		–0.54	
Gepang Gath	2016–17		–1.50	
	2017–18		–1.51	
Pensilungapa	2016–17	Glaciological	–0.23	
	2017–18		–0.56	
Samundra Tapu	2016–17		–1.12	
	2017–18		–1.56	
Sutri Dhaka	2016–17		–0.87	
	2017–18		–1.34	
Siachen	1987–91	Hydrological	–0.48 to –1.084	55

AAR, Accumulation area ratio; TI, Temperature index.

mass balance of glaciers at a high temporal resolution¹⁹, which can then be scaled to basin-wide mass balance^{13,15,28–30}. A regression equation was developed by Kulkarni *et al.*¹⁷ between AAR and specific mass balance using field data for the Gor Garang glacier (1976–1984) and Shaune Garang glacier (1982–1988). To calculate AAR, knowledge about equilibrium line of altitude (ELA) is required, which is derived by interpolating field-specific mass balance to the altitude of zero mass balance³¹. In India, *in situ* mass balance data are limited and available for a few glaciers only due to the rugged Himalayan terrain¹⁹. However, satellite data are being used to derive the transient snowline at the end of hydrological year which coincides with ELA for a temperate glacier^{29,32,33}. Hence, studies reported in different parts of the Himalaya used transient snow line from satellite images to derive AAR and mass balance^{34–36}. To overcome the challenges of identifying ELA from satellite images, Tawde *et al.*¹⁵ developed an approach by calculating TSL using degree day/temperature index (DD/TI) model¹⁴. The resultant model-derived TSL and AAR were in the regression equation developed for the basin to estimate mass balance at the glacier as well as basin scale. This improved AAR (IAAR) method has been applied for the Chandra basin, which suggests regional-scale negative mass balance of -0.61 ± 0.46 m.w.e./year (ref. 15). Mass balance derived for glaciers in the Chandra basin using the IAAR equation correlate well with *in situ* specific mass balance reported by Azam *et al.*⁶ and Wagnon *et al.*³⁷. Hence the IAAR method has been adopted in this study to estimate AAR and regressed mass balance for the Bhaga basin. Mass balance for various glaciers of the Himalaya reported using different methods is given in Table 1, which shows that majority of the glaciers are losing mass and thinning subsequently from 1990 onwards.

Study area

Bhaga, a sub-basin of Chenab basin (Figure 1), is situated in the north of Pir Panjal range at Lahaul and Spiti valley, Himachal Pradesh, India ($32^{\circ}28'19.7''N$ – $33^{\circ}0'9.9''N$ and $76^{\circ}56'6.3''E$ – $77^{\circ}25'23.7''E$) covering an area of 1684 sq. km. The Bhaga river originating from Suraj Tal lake joins the Chandra river at Tandi (2950 m amsl). Jankar Nala and Milang river join the Bhaga at an altitude of 3307 m amsl at Darcha Dangma, a village near the Bhaga basin.

The importance of the Bhaga basin lies in the fact that this region falls under the monsoon – arid transition zone marking the boundary between wet climate in the south and dry climate in the north. South Asian monsoons in summer and the westerlies in winter influences glaciers of the Bhaga basin¹⁸.

This region is bounded by high peaks from all sides with most of the glaciers of the Bhaga basin located on the Leh–Manali highway. The Bhaga basin consists of 231 glaciers with slope ranging between 5° and 25° (Figure 2; ref. 14). Nine glaciers of the Bhaga basin were selected for the present study based on topography (elevation, orientation, area, length, slope) and cloud-free satellite data availability (Table 2). Two unnamed glaciers with GLIMS ID G077301E32493N and G076977E32847N are named as Karparaikal (heavy debris-covered) and Shadvakra (six tributary glaciers joining the central flow line) respectively, in this study.

Methodology

Data used

Meteorological data: The present study utilizes meteorological data of daily temperature and precipitation

Table 2. Topographic characteristics of nine selected glaciers indicating area, aspect/orientation, mean altitude and slope. The selected glaciers cover an area of 125.50 sq. km with Mulkila being the largest benchmark glacier of the Bhaga basin

Basin	Glacier	Area (sq. km)	Aspect/orientation	Mean altitude (m)	Slope (degree)
Bhaga	Patsio	2.61	15/N	4549	21
	Panchinala	6.40	10/N	4997	16
	Mulkila	30.35	310/NW	4884	22
	Bugsubgang	5.74	317/NW	5000	33
	Kelasbung	7.50	123/SE	5363	16
	Gangstang	22.60	7/N	5220	17
	Shadvaktra	15.09	26/N	5354	15
	Lady of Keylong	13.21	100/SE	6061	16
	Karparaikal	22.00	287/NW	4624	15

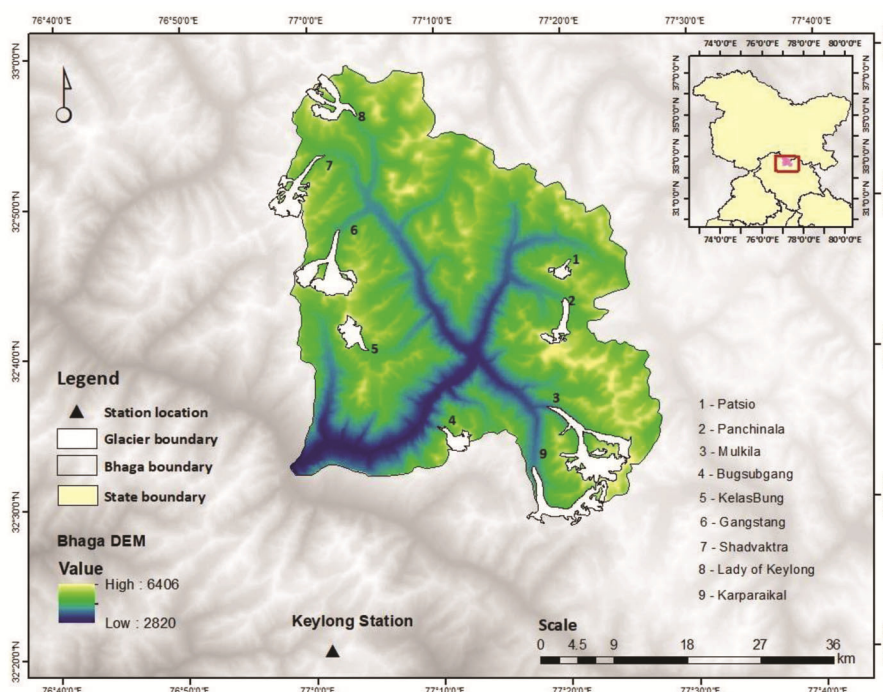


Figure 1. Map of Bhaga basin, Western Himalaya showing the location of the selected glaciers. Bhaga basin has a glaciated area of 351.89 sq. km. Colour scale indicates elevation details of the basin. *In situ* data-recording AWS station in Keylong, Himachal Pradesh (3120 m amsl) is indicated by a triangle.

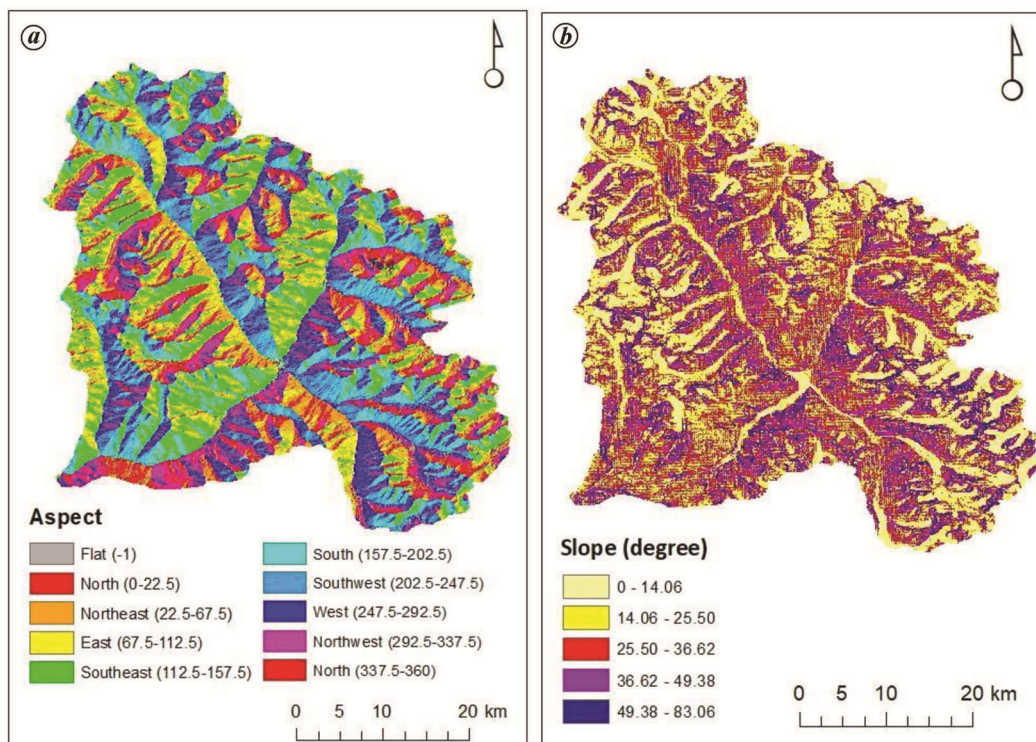
recorded using AWS installed at Keylong, Himachal Pradesh (32°20'24"N and 77°01'12"E) at an elevation of 3120 m amsl by India Meteorological Department (IMD). *In situ* data include minimum, maximum and average temperatures (°C) along with rainfall and snowfall data (mm) on a daily basis for the period 2008–2018.

Remote sensing data: Landsat 7 (Enhanced Thematic Mapper plus), Landsat 8 (Operational Land Imager) and Sentinel 2 A & B (multi spectral instrument) with minimum cloud cover (less than 10%) were used for identification of transient snowline (TSL; Table 3). Landsat 7 datasets acquired after 31 May 2003 contain scan-line errors due to failure of on-board scan-line corrector.

Scan-line error corrections have been carried out using GDAL_nodatafill tool of Quantum Geographic Information System (QGIS 3.4.4.), which is a free and open-source cross-platform application. This tool calculates the surrounding pixel values with the help of an inverse distance weighting algorithm. The spatial resolution of Landsat 7/8 data is 15–60 m, with a temporal resolution of 16 days. Sentinel 2 (A & B) data have a spatial resolution of 10–60 m, with a temporal resolution of 10 days. Combined revisit period of Sentinel 2 A & B is five days. In total, 61 images (45 images from Landsat 7/8 and 16 images from Sentinel 2) for a study period 2008–2018 were processed. The year 2010 was not included due to unavailability of cloud-free data. ALOS PALSAR (Advanced

Table 3. Spatial resolution and acquisition details of satellite data used in this study. Landsat 7/8 data require preprocessing as they are available in the form of digital numbers

Satellite	Spatial resolution (m) and band used	Year/path and row
Landsat 7	30; band 2 (green), band 4 (NIR) and band 5 (SWIR)	2008–11; 147/37
Landsat 8	30; Band 3 (green), band 5 (NIR) and band 6 (SWIR)	2012–16; 147/37
Sentinel 2 (A and B)	10; Band 3 (green) band 8 (NIR) and band 11 (SWIR)	2017–18; R105, T43SFS/T43SGS
ALOS PALSAR DEM	30 and 12.5	High-resolution and low-resolution digital elevation model

**Figure 2.** Bhaga basin. *a*, Aspect map showing the direction of physical slope face. *b*, Slope map showing the degree of inclination relative to the horizontal plane.

Land Observing Satellite Phased Array L-band Synthetic Aperture Radar) – Radiometrically Terrain-Corrected (RTC) Digital Elevation Model (DEM) products with a spatial resolution of 12.5–30 m from the Alaska satellite facilities were used. Glacier boundaries available from Randolph Glacier Inventory (RGI V 6.0.)³⁸ were manually modified for delineation of glaciated area from satellite images.

Data processing

The present study is based on the IAAR model proposed using *in situ* and satellite data. Data processing was carried out for the selected nine glaciers of the Bhaga

basin in the following phases (Figure 3): (i) Preprocessing of satellite data and identification of transient snow line (TSL_{sat}), (ii) Calculation of total melt during summer for every 50 m elevation interval, (iii) Estimation of vertical precipitation gradient and total accumulation during winter for every 50 m elevation interval. (iv) Model-derived transient snow line (TSL_{mod}) and AAR calculation. For the present study, October to May (243 days) and June to September (122 days) were considered for calculating accumulation and ablation respectively, for a given hydrological year¹⁵.

Preprocessing of data: Sentinel 2 Level 1C top of atmospheric (TOA) data product is available with radiometric and geometric corrections at sub-pixel accuracy.

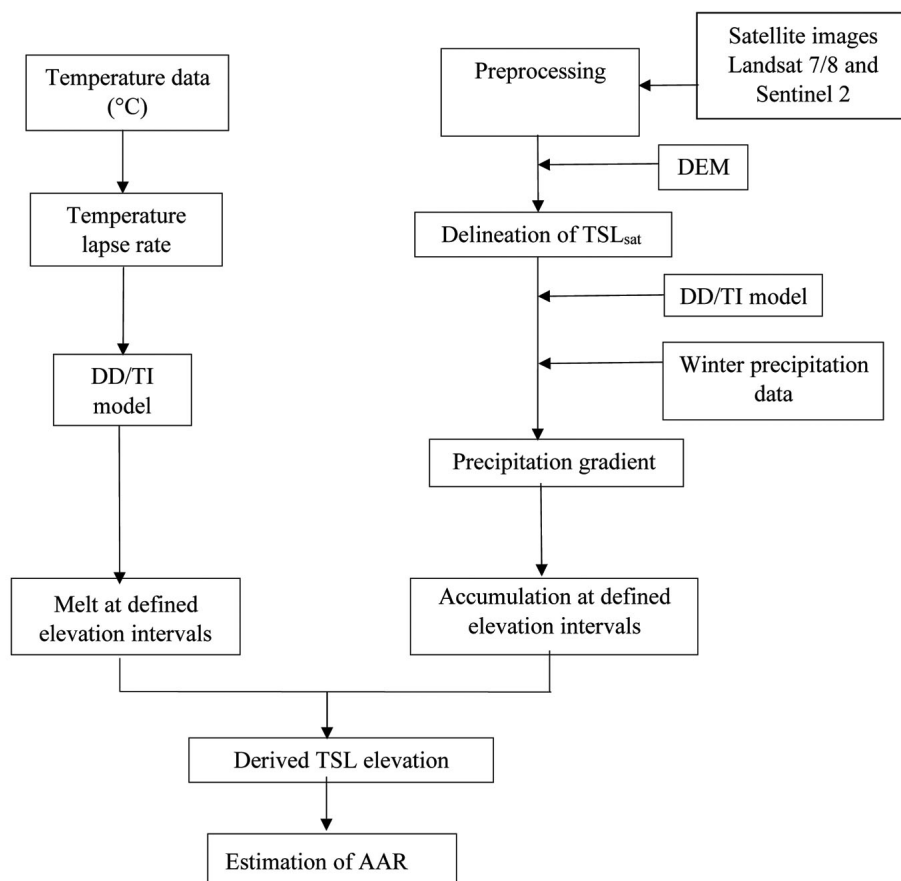


Figure 3. Flow chart showing the data processing adopted for the present study. It includes: (i) Preprocessing of data and identification of transient snow line (TSL_{sat}) from multispectral satellite images; (ii) calculation of total melt during summer at every 50 m elevation interval; (iii) estimation of vertical precipitation gradient and total accumulation during winter at every 50 m elevation interval and (iv) Model-derived transient snow line (TSL_{mod}) and accumulation area ratio (AAR) calculation.

Landsat 7 and 8 images are available in the form of digital numbers (DN) to the users from the US Geological Survey (USGS) website. The images are radiometrically corrected by converting DN to radiance and to TOA in preprocessing³⁹.

Identification of transient snow line from satellite images

For identification and delineation of TSL_{sat} , TOA reflectance data obtained from preprocessing of satellite images were used. It is important to distinguish between snow-covered accumulation region and ice-exposed ablation region to map the TSL_{sat} of a glacier, which is used for calculating precipitation gradient. False colour composite (FCC) images of green, near infrared (NIR) and shortwave infrared (SWIR) bands of Landsat 7/8 and Sentinel 2 data were used to differentiate between snow and ice (Figure 4). Nearest neighbour resampling algorithm was used in Sentinel 2 SWIR band to convert the resolution to 10 m. Snow has a high and low spectral

response in visible and infrared bands respectively, which makes FCC (green, NIR and SWIR) images suitable for the identification of TSL_{sat} .

Calculation of melt during summer (June–September)

Temperature (T_h) at an average altitude of every 50 m elevation interval was calculated with base station temperature data and temperature lapse rate using eq. (1). Using eq. (2), positive degree days (PDD) were calculated from T_h . Ablation melt for every 50 m elevation interval was computed using eqs (3) and (4) with a snowmelt factor of $4 \text{ mm } ^\circ\text{C}^{-1} \text{ day}^{-1}$ (ref. 14) from 1 June to 30 September (122 days).

$$T_h = T_0 + \text{TLR} * \Delta h, \quad (1)$$

where h is the average altitude of every 50 m elevation interval, T_h the temperature at elevation h ($^\circ\text{C}$), T_0 the temperature at the base station ($^\circ\text{C}$), TLR the temperature

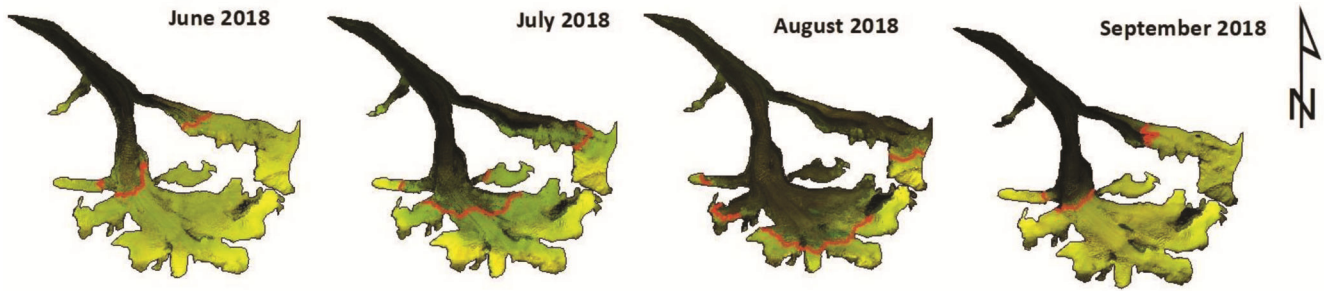


Figure 4. Identification of TSL of Mulhila glacier from satellite images for the ablation period (June–September) during hydrological year (HY) 2017–2018. TSL at the highest altitude is observed in August 2018. TSL shifted to mid altitude in September 2018, which may be due to snowfall.

lapse rate ($^{\circ}\text{C}/\text{km}$) and Δh is the elevation difference of base station and h .

$$\text{PDD} = \begin{cases} 0 & \text{for } T_h < 0 \\ T_h & \text{for } T_h > 0 \end{cases} \quad (2)$$

$$S_c = \sum_{i=1}^n \text{SMF} * \text{PDD}, \quad (3)$$

where S_c is the melt (mm/day) at elevation h and SMF the snowmelt factor

$$CS_c = S_c * 122 \text{ days}, \quad (4)$$

where CS_c is the cumulative melt (mm) for summer period at elevation h .

Calculation of precipitation gradient, total accumulation and model-derived TSL

Mass balance at ELA is zero. As melt balances the accumulation at ELA⁴⁰, TSL altitude is assumed as a proxy of ELA¹⁹. This definition forms the basis for calculating precipitation gradient and total accumulation for every 50 m elevation interval using eqs (5) and (6).

$$P_g \% = \frac{P_T - P_S}{(h_T - h_S) * P_S} * 100, \quad (5)$$

where P_g is the precipitation gradient ($\% \text{m}^{-1}$) between elevation of TSL_{sat} and meteorological station; P_T the precipitation at the TSL_{sat} , P_S the precipitation recorded at the base station, h_T the elevation of TSL_{sat} and h_S is the elevation of the meteorological station.

$$A_c = P_0 + (P_g * \Delta h), \quad (6)$$

where A_c is the cumulative accumulation, P_0 the station precipitation data and Δh is the elevation difference of h and the station.

The elevation at which the cumulative ablation in summer balances the cumulative accumulation in winter

is considered as model-derived transient snow line (TSL_{mod}) elevation for that particular year. Altitudinal distribution of accumulation area and ablation area of glaciers was calculated using precipitation gradient and temperature data obtained from AWS. The 50 m elevation interval at which ablation balances accumulation was considered for estimating model-derived TSL. The model-derived transient snow line (TSL_{mod}) elevation agreed remarkably well with TSL_{sat} obtained from satellite images, which were then used to calculate AAR. Area covered under this particular 50 m elevation interval was then averaged and distributed between accumulation and ablation regions for AAR estimation.

Uncertainties

Delineation of snow line manually from satellite data introduces a small degree of uncertainty during the calculation of TSL and AAR. For calculation of accumulation and ablation area, 50 meter elevation bins were generated using DEM. The elevation bin at which the accumulation balances ablation was considered for calculation of modelled TSL. Area covered by the respective elevation bin was proportioned between the accumulation and ablation regions. This can cause an overestimation or underestimation of AAR within negligible range¹⁵. The uncertainty z was estimated using eq. (7).

$$\delta z = \sqrt{\left(\frac{\partial Z}{\partial T} \delta T\right)^2 + \left(\frac{\partial Z}{\partial P} \delta P\right)^2 + \left(\frac{\partial z}{\partial \gamma} \delta \gamma\right)^2 + \left(\frac{\partial z}{\partial P_{\text{grad}}} \delta P_{\text{grad}}\right)^2 + \left(\frac{\partial z}{\partial \rho} \delta \rho\right)^2}, \quad (7)$$

where δP_{grad} , δT , $\delta \gamma$ and δP are the uncertainties measured from precipitation gradient (P_{grad}), temperature (T), temperature lapse rate (γ) and precipitation (P) respectively. As the Chandra basin is adjacent to the Bhaga basin, the standard values reported for the former were adopted in eq. (14) for uncertainty calculation. For a ± 210 m variation of TSL estimation, the percentage of

change in AAR was observed to be approximately 19. Figure 5 represents standard error in the range 2–5% for estimated mean mass loss obtained from eqs (9)–(12) for the nine glaciers.

Results and discussion

Equilibrium line of altitude

ELA is a glacier’s most fundamental feature that divides it into accumulation and ablation zones⁴¹. As the glacier retreats, ELA shifts upwards with altitude, which helps us understand that the glacier is retreating. Moreover, ELA is a suitable but not precise method to analyse changes in a glacier⁴². Overall, 61 satellite images have been used to delineate TSL (which is the proxy of ELA) for the ablation period 2008–2018. The Bhaga basin is covered by two different orbits of Sentinel 2 satellites. Sixteen images of Sentinel 2 were merged into eight images to obtain the study area for the ablation period of 2016–2018. A total of 424 transient snow lines have been delineated from 61 satellite images of Landsat 7/8 and Sentinel 2 A and B for the study period. Figure 6 shows the monthly

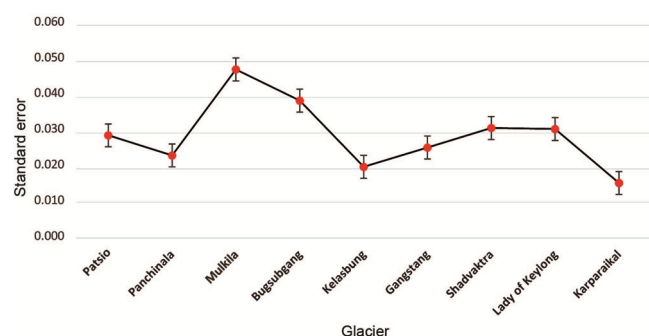


Figure 5. Standard error of mean mass loss calculated from the regression equations, viz. eqs (9)–(12).

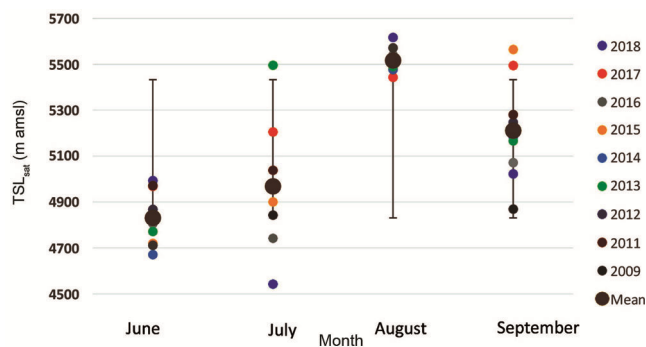


Figure 6. Average elevation of satellite-derived TSL during ablation time from 2008 to 2018. The colour dots represent position of TSL in each year. The vertical bar represents standard deviation in the snow-line altitude. *Year 2010 not included due to satellite data gap.

averaged snow line altitude estimated for the nine glaciers of the Bhaga basin. It is observed that mean altitude of snow line increases progressively from 4831 ± 124 m amsl in June to 4968 ± 290 m amsl in July. Maximum altitude of 5516 ± 53 m amsl was observed in August. In September, mean elevation of transient snow line was 5210 ± 219 m amsl which decreased by 306 m compared to August. The standard error estimated in the satellite-derived snow line was approximately ± 171 m. The variations in mean altitude of snow line from glacier to glacier indicate that every glacier and its response to environmental factors are different. It has been also reported that due to topography¹⁸ and variations in temperature as well as precipitation²⁵, snowline altitude varies with each glacier.

In order to compare satellite-derived TSL and model-derived TSL, $\Delta TSL = (TSL_{sat} - TSL_{mod})$ was calculated. Average ΔTSL falls within ± 150 m (Figure 7). Analysis of TSL_{sat} suggests that altitude of snow line will be lowest at the beginning of the ablation period (June) due

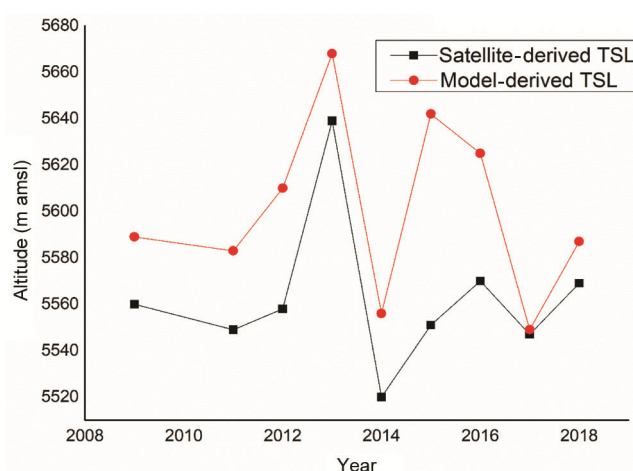


Figure 7. Satellite-derived TSL (TSL_{sat}) and modelled TSL (TSL_{mod}) calculated for the selected nine glaciers averaged for each year. $\Delta TSL = (TSL_{sat} - TSL_{mod})$ falls within ± 150 m for the study period. *Year 2010 not included due to satellite data gap.

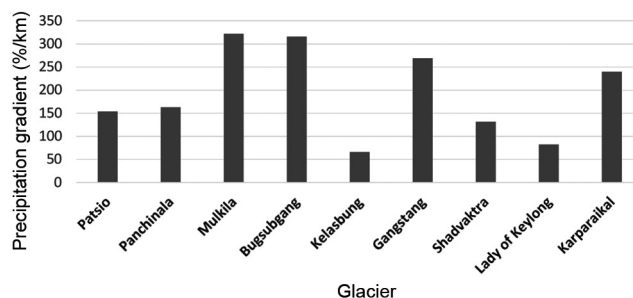


Figure 8. Estimated precipitation gradient ($\% \text{ km}^{-1}$) for the nine glaciers represented as vertical bars. Kelasbung and Lady of Keylong exhibit low precipitation gradient as they are situated on the leeward side of the westerlies.

to the presence of snow. TSL_{sat} gradually increases due to melting of snow and reaches its maximum altitude at the end of the ablation season (September). According to Azam *et al.*⁶, the melt season extends up to September end or first week of October. For the present study, satellite-derived TSL (at higher elevation) for the study area occurred in August, which is considered as ELA for the calculation of AAR. The melt season extended till the end of September, when *in situ* measurements were taken. Hence, decline in elevation of satellite-derived TSL was observed during September, possibly due to fresh snowfall¹³.

Precipitation gradient

The precipitation gradient was calculated from 72 highest averaged TSL altitudes (Figure 8), which varied from 66% to 322% km^{-1} . The mean precipitation gradient for the nine selected glaciers was calculated as approximately $193 \pm 93\% km^{-1}$ or $379 \pm 113 mm km^{-1}$ at 60th percentile, indicating distortion in the distribution. For calculation mean precipitation gradient, winter cumulative precipitation for study period 2008–2009 and 2011–2018 was considered. Since the regional topography of the glacier controls precipitation of the region, standard deviation of the precipitation gradient was higher³⁰. A positive correlation of 0.67 was observed between the slope and precipitation gradient of glaciers, which is possibly due to steep slopes facing the westerlies. For the Chandra basin situated next to the Bhaga basin, a positive correlation of 0.65 has been reported¹⁵. Precipitation gradient of the Chandra basin obtained from the Kaza station (3600 m amsl) correlates well with that of the Bhaga basin, which has been estimated from Keylong station (3120 m amsl) data. Southeast-facing glaciers (Kelasbung and Lady of Keylong) have low precipitation gradient possibly because they are situated in the leeward side of the westerlies. North (Patsio, Panchinala, Gangstang, Shadvaktra) and northwest (Mulakila, Bugsubgang and Karparaikal) glaciers show a high precipitation gradient, probably because they are located in the windward side of the western disturbances.

Modelled accumulation area ratio

To estimate conventional AAR, satellite-derived TSL was used. TSL was projected on a hypsometric curve for a given glacier, where the area above and below the TSL represents the accumulation and ablation region respectively. Glacier shapefiles from RGI V.6.0 were modified manually to estimate glacier area using open source QGIS software to compute glacier hypsometry. Figure 9 represents the hypsometry curve of Mulakila glacier. Similarly, hypsometry for all nine glaciers were computed for AAR calculation. From eq. (8), modelled AAR for the

nine glaciers was computed from DD/TI method using modelled TSL. Mean modelled AAR and conventional AAR lie in the range 10–30% and 10–34% respectively, for the nine glaciers (Figure 10). Glaciers like Mulakila, Panchinala, Lady of Keylong, Patsio and Karparaikal have debris-covered ablation region with low AAR values¹⁶. The variability in AAR can be related to the diverse behaviour of glaciers and limitations in the availability of meteorological data from more than one station. Basin-wide mean AAR was observed to be 0.5 ± 0.06 , which varied by 10% in comparison with conventional AAR of 0.4 ± 0.04 .

$$AAR = \frac{\text{Accumulation area}}{\text{Total glacier area}} \quad (8)$$

Figure 11 shows year-wise AAR for Mulakila glacier. The variations observed between conventional AAR and modelled AAR were around 20% for 2011, 2012, 2016 and 2018 followed by 10% for 2017 and 5% for 2009 and 2014. This study suggests that model-based TSL and AAR can be used as an alternative to the satellite-derived TSL and AAR, with a standard error of 12–16%.

Large AAR value indicates that the glacier ice is covered with snow, protecting the ice from melting due to exposure. When the glacier remains snow-covered, melting of snow results in lesser mass loss due to density difference between snow and ice. AAR of smaller value indicates that large area of bare ice is exposed resulting in increased mass loss. Hence, AAR is one of the crucial parameters in assessing glacier health.

AAR and mass balance

Annual mass balance (MB) for a glacier or at regional basin scale can be estimated with regression equations

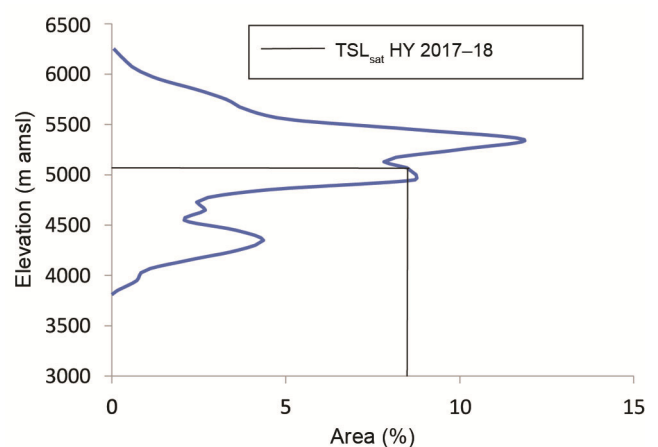


Figure 9. Hypsometry curve for Mulakila glacier derived using ALOS PALSAR DEM representing percentage of glacier area with respect to elevation. For representation purpose, TSL of HY 2017–2018 has been projected on the hypsometry.

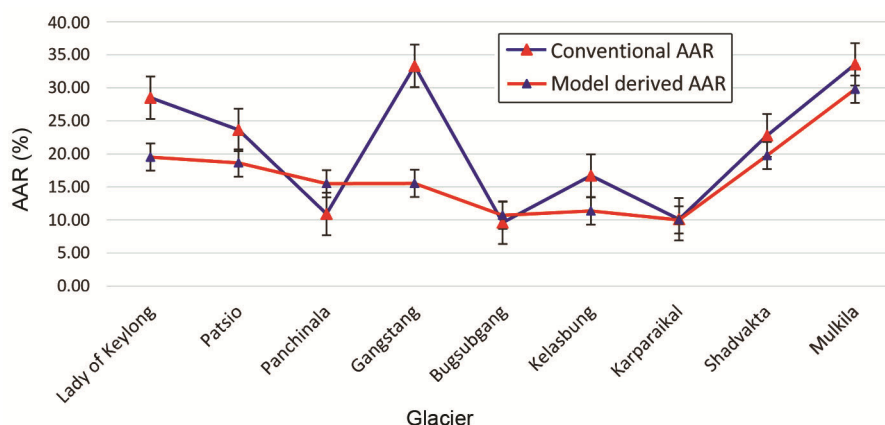


Figure 10. Mean AAR of nine glaciers for 2008–2009 and 2011–2018 using conventional and DD/TI methods. The vertical bar represents standard deviation in AAR calculation. Model-derived AAR of Gangstang is an underestimation when compared with conventional AAR.

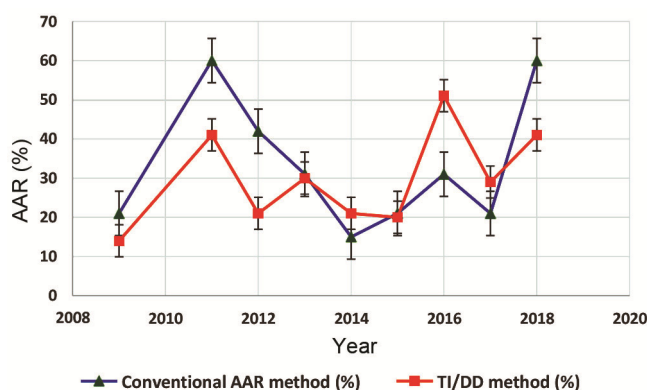


Figure 11. AAR calculated for Mukkila glacier from 2008–2009 and 2011–2018, using conventional and DD/TI method. The vertical bar represents standard deviation in AAR calculation.

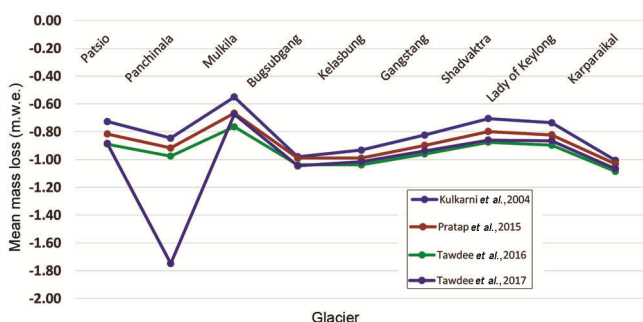


Figure 12. Regressed mean mass loss for the nine selected glaciers in Bhaga basin using different equations from the literature.

relating AAR and field mass balance. Different regression eqs (9) to (12) available in the literature have been used to calculate mass balance of the nine glaciers (Figure 12) and the Bhaga basin. Equation (9) was developed by Kulkarni *et al.*¹⁷ for Shaune Garang and Gor-Garang glaciers in Himachal Pradesh based on field

estimates of mass balance and satellite-derived AAR from 1982 to 1988 and 1976 to 1984 respectively. Equation (11) has been subsequently modified as eq. (12) for the Western Himalaya by Pratap *et al.*⁴² using four decades of mass balance observations of ten glaciers in the region since 1970. Regression equation, viz. eq. (12) has been developed for the Chandra basin using modelled AAR and field mass balance of Chhota Shigri from 1987–1989 to 2002–2009. Equation (11) has been improved into eq. (12) with data available from 1987–1989 to 2002–2012 (ref. 13).

$$MB = 243.01 * AAR - 120.187, \tag{9}$$

$$MB = 205.7 * AAR - 121.8, \tag{10}$$

$$MB = 174.6 * AAR - 123.2, \tag{11}$$

$$MB = 186.3 * AAR - 122.8, \tag{12}$$

Only limited studies on glacier mass balance are available in the literature for the Bhaga basin. Angchuk *et al.*⁴³ and Kuhn⁴⁰ have reported the mass balance of Patsio glacier using glaciology (2012–2013) and geodetic (2000–2013) methods respectively. Average mass loss for the Bhaga basin was estimated as approximately -0.98 , -1.03 , -1.074 and -1.06 m.w.e.a⁻¹ using eqs (9–12) respectively. Variations in mass balance of the nine glaciers shown in Figure 12 can be possibly due to distinct behaviour of these glaciers and limitations in the application of different regression equations⁴⁴. Considering modelled mass balance obtained from IAAR (eq. (12)), it can be observed that irrespective of glacier size, small and large glaciers have undergone a considerable amount of thinning around -7.74 ± 0.3 to -9.06 ± 0.45 m.w.e., except for the Mukkila glacier (-6.07 ± 0.5 m.w.e) during the study period. The Karparaikal glacier of an area 22.04 sq. km, which is heavily debris-covered from snout to middle

Table 4. Comparison of mass balance of Patsio glacier using different methods

Glacier	Year	Present study (m.w.e./year)	Geodetic method (m.w.e./year)	Glaciological method (m.w.e.)
Patsio	2012–13	-1.14 ± 0.30	-0.26 ± 0.11	0.04 ± 0.40
	2015–16	-0.92 ± 0.30	–	–0.68
	2016–17	-1.15 ± 0.30	–	–0.45

Table 5. Details of *in situ* data collected

Glacier ID	RGI50-14.12673
Glacier type	Debris-free glacier
Basin	Indus
Date of validation	18 August 2018
Model-derived transient snow line (TSL) (a)	5344 m amsl
<i>In situ</i> measured TSL using GNSS survey (b)	5331 m amsl
Difference (a)–(b)	13 m amsl

**Figure 13.** Field photographs indicating mapping of snow-line elevation using spectra precision SP80 DGPS in static mode.

accumulation region, has a cumulative mass loss of -9.06 m.w.e. with a standard error of ± 0.09 . Mass loss obtained from AAR methods for heavy debris-covered glaciers may sometimes result in overestimation of mass loss.

Patsio glacier mass balance analysis

Annual mass balance measured for the Patsio glacier by glaciological method showed positive mass balance of 0.04 ± 0.40 m.w.e. during 2012–2013 (ref. 51) and negative mass balance of -0.68 and -0.45 m.w.e during 2015–2016 and 2016–2017 respectively⁴⁵. Geodetic based mass balance for Patsio glacier for the period 2000–2013 reports thinning of the glacier with negative mass balance

of -0.26 ± 0.11 m.w.e. a^{-1} . Mass balance from model-based AAR (eq. (12)) for the Patsio glacier was compared with geodetic and glaciological-based mass balance (Table 4). Model-based mass balance of -1.14 ± 0.30 m.w.e. for 2012–2013, -0.92 ± 0.30 m.w.e. for 2015–2016 and -1.15 ± 0.30 m.w.e. for 2016–2017 was found to be an overestimation compared to other methods. This may be possibly due to the following reasons: (a) spatial interpolation of specific mass balance, (b) limitations of InSAR (synthetic aperture radar interferometry)-based DEMs for mountainous terrain and combining DEMs of different sensors/techniques (photogrammetry and InSAR-based) and spatial resolution, (c) mass balance of a glacier or a basin averaged over the study period and (d) application of regression equations relating AAR and mass balance developed for different glaciers.

Field-based TSL

The method of estimating satellite-derived and model-derived AAR and TSL was validated on a debris-free glacier with glacier ID RGI 5.0–14.12673 near Khardhungla, Leh (Figure 13). Validation was carried out on 18 August 2018 in synchronization with satellite data acquisition using DGPS (differential global positioning system) of spectra Precision SP80. TSL and snout of the glacier were mapped using static mode of GNSS (global navigation satellite system) survey. GNSS base unit was set for an occupation time, a minimum of 10 h to achieve the desired level of accuracy. Post-processing of GNSS data was carried out with Spectra Precision Survey office ver. 4.10.3. Individual snow-line elevation points obtained from the field and satellite image were averaged to estimate the mean TSL altitude. From Table 5, it can be observed that the *in situ* measured TSL altitude matches well with the model-derived TSL altitude of the glacier, making the methodology of the present study more robust. The appropriateness of the proposed methodology to estimate modelled mass balance has been assessed with field estimates of Chhota Shigiri during 1999–2011 (ref. 15).

Conclusion

Field data of mass balance are available for only a few glaciers of the Himalaya, as they are least explored due to harsh climate and inaccessibility to glaciers. Hence, in

this study we calculate glacier mass loss using different regression equations developed based on field estimates of mass balance and AAR. Mass balance, TSL and AAR have been calculated using satellite data, meteorological data and model-based improved AAR method for nine selected glaciers of the Bhaga basin. Using IAAR method, the mean mass loss calculated for the nine glaciers of the Bhaga basin was $-1.01 \pm 0.3 \text{ m.w.e. a}^{-1}$, with basin-wide mean mass loss of $-1.06 \pm 0.03 \text{ m.w.e. a}^{-1}$ for 2008–2009 and 2011–2018. Results indicate that glaciers of the Bhaga basin have undergone significant amount of mass loss and thinning during the study period. Also, it has been observed that estimation of mass loss for a specific glacier varies with altitude, size, shape, temperature and other environmental factors. Synergetic use of meteorological data which are available throughout the year, makes the present method and study more robust for the Himalayan glaciers.

1. Bolch, T. *et al.*, The state and fate of Himalayan glaciers. *Science*, 2012, **336**, 310–314.
2. Kulkarni, A. V. and Karyakarte, Y., Observed changes in Himalayan glaciers. *Curr. Sci.*, 2016, **106**(2), 237–244.
3. Kulkarni, A. V. and Buch, A. M., *Glacier Atlas of Indian Himalaya*, SAC/RSA/RSAG- MWRD/SN/05/91, 1991, p. 62.
4. Bookhagen, B. and Burbank, D. W., Toward a complete Himalayan hydrological budget: spatiotemporal distribution of snowmelt and rainfall and their impact on river discharge. *J. Geophys. Res.*, 2010, **115**(F3), F03019; doi:10.1029/2009JF001426.
5. Puri, M. and Thakur, P. K., Remote sensing based accumulation area ratio method for glacier mass balance of Chhota Shigri Glacier. *IJARST*, 2015, **4**(1), 171–184.
6. Azam, M. F., Wagon, P., Vincent, C., Ramanathan, A. L., Favier, V., Mandal, A. and Pottakkal, J. G., Processes governing the mass balance of Chhota Shigri Glacier (western Himalaya, India) assessed by point-scale surface energy balance measurements. *Cryosphere*, 2014, **8**, 2195–2217.
7. Gaddam, V. K., Kulkarni, A. V. and Gupta, A. K., Assessment of the Baspa basin glaciers' mass budget using different remote sensing methods and modeling. *Geocarto Int.*, 2018, **35**(3), 296–316.
8. Azam, M. F., Wagon, P., Berthier, E., Vincent, C., Fujita, K. and Kargel, J. S., Review of the status and mass changes of Himalayan–Karakoram glaciers. *J. Glaciol.*, 2018, **64**(243), 61–74.
9. Barnett, T. P., Adam, J. C. and Lettenmaier, D. P., Potential impacts of a warming climate on water in snow-dominated regions. *Nature*, 2005, **438**, 303–309.
10. Chaturvedi, R. K., Kulkarni, A. V., Karyakarte, Y., Joshi, J. and Bala, G., Glacial mass balance changes in the Karakoram and Himalaya based on CMIP5 multi-model climate projections. *Climate Change*, 2014, **123**(2), 315–328.
11. Fischer, A., Comparison of direct and geodetic mass balances on a multi-annual time scale. *Cryosphere*, 2011, **5**, 107–124.
12. Immerzeel, W. W., van Beek, L. P. H., Konz, M., Shrestha, A. B. and Bierkens, M. F. P., Hydrological response to climate change in a glacierized catchment in the Himalayas. *Climate Change*, 2012, **110**, 721–736.
13. Tawde, S. A., Kulkarni, A. V. and Bala, G., An estimate of glacier mass balance for the Chandra basin, Western Himalaya, for the period 1984–2012. *Ann. Glaciol.*, 2017, **58**(75), 99–109.
14. Huss, M., Sold, L., Hoelzle, M., Stokvis, M., Salzmann, N., Farinotti, D. and Zemp, M., Towards remote monitoring of sub-glacier mass balance. *Ann. Glaciol.*, 2013, **54**(63), 85–93.
15. Tawde, S. A., Kulkarni, A. V. and Bala, G., Estimation of glacier mass balance on a basin scale: an approach based on satellite-derived snowlines and a temperature index model. *Curr. Sci.*, 2016, **111**(12), 1977–1989.
16. Birajdara, F. S., Venkataramana, G., Bahugunab, I. M. and Samant, H. P., A revised glacier inventory of Bhaga basin, Himachal Pradesh, India: current status and recent glacier variations. *ISPRS Ann. Photogramm., Remote Sensing Spat. Infor. Sci.*, 2014, **II-8**, 37–43.
17. Kulkarni, A. V., Rathore, B. P. and Alex, S., Monitoring of glacial mass balance in the Baspa basin using accumulation area ratio method. *Curr. Sci.*, 2004, **86**(1), 185–190.
18. Pandey, P., Kulkarni, A. V. and Venkataraman, G., Remote sensing study of snowline altitude at the end of melting season, Chandra-Bhaga basin, Himachal Pradesh, 1980–2007. *Geocarto Int.*, 2013, **28**(4), 311–322.
19. Kulkarni, A. V., Mass balance of Himalayan glaciers using AAR and ELA methods. *J. Glaciol.*, 1992, **38**(128), 101–104.
20. Dobhal, D. P., Mehta, M. and Srivastava, D., Influence of debris cover on terminus retreat and mass changes of Chorabari Glacier, Garhwal region, central Himalaya. *Indian J. Glaciol.*, 2013, **59**(217), 961–971.
21. Gardelle, J., Berthier, E., Arnaud, Y. and Käab, A., Region-wide glacier mass balances over the Pamir–Karakoram–Himalaya during 1999–2011. *Cryosphere*, 2013, **7**(4), 1263–1286.
22. Vijay, S. and Braun, M., Elevation change rates of glaciers in the Lahaul–Spiti (western Himalaya, India) during 2000–2012 and 2012–2013. *Remote Sensing*, 2016, **8**(12), 1–16.
23. Käab, A., Berthier, E., Nuth, C., Gardelle, J. and Arnaud, Y., Contrasting patterns of early 21st century glacier mass change in the Himalaya. *Nature*, 2012, **488**(7412), 495–498.
24. Chandrasekharan, A., Ramsankaran, R. A. A. J., Pandit, A. and Rabatel, A., Quantification of annual glacier surface mass balance for the Chhota Shigri Glacier, Western Himalayas, India using an equilibrium-line altitude (ELA) based approach. *Int. J. Remote Sensing*, 2018, **39**(23), 9092–9112.
25. Anant Kumar, Negi, H. S., Kumar, K., Kanda, N. and Singh, K. K., Estimation of recent changes in thickness and mass balance of the Patsio glacier in Great Himalayan region using geodetic technique and ancillary data. *Geocarto Int.*, 2018, **35**(1), 47–63.
26. Matsuo, K. and Heki, K., Time-variable ice loss in Asian high mountains from satellite gravimetry. *Earth Planet. Sci. Lett.*, 2010, **290**, 30–36.
27. Jacob, T., Wahr, J., Pfeffer, W. and Swenson, S., Recent contributions of glaciers and ice caps to sea level rise. *Nature*, 2012, **482**, 514–518.
28. Kulkarni, A. V., Effect of climatic variations on Himalayan glaciers: a case study of upper Chandra River basin, Himachal Pradesh. In Paper presented at the Indo-US Symposium–Workshop on Remote Sensing and its Application, Mumbai, 1996.
29. Rabatel, A., Letréguilly, A., Dedieu, J. P. and Eckert, N., Changes in glacier equilibrium-line altitude in the western Alps from 1984 to 2010: evaluation by remote sensing and modeling of the morpho-topographic and climate controls. *Cryosphere*, 2013, **7**(5), 1455–1471.
30. Braithwaite, R. and Raper, S., Estimating equilibrium-line altitude (ELA) from glacier inventory data. *Ann. Glaciol.*, 2009, **50**(53), 127–132.
31. Kaser, G., Fountain, A. and Jansson, P., A manual for monitoring the mass balance of mountain glaciers, IHP–VI. Technical Documents in Hydrology, UNESCO, Paris, 2003.
32. Cogley, J. G., Geodetic and direct mass-balance measurements: comparison and joint analysis. *Ann. Glaciol.*, 2009, **50**(50), 96–100.
33. Bamber, J. L. and Rivera, A., A review of remote sensing methods for glacier mass balance determination. *Global Planet. Change*, 2007, **59**(1–4), 138–148.

34. Arora, M., Singh, P., Goel, N. K. and Singh, R. D., Spatial distribution and seasonal variability of rainfall in a mountainous basin in the Himalayan region. *Water Resour. Manage*, 2006, **20**(4), 489–508.
35. Brahmabhatt, R. M., Bahuguna, I., Rathore, B. P., Kulkarni, A. V., Shah, R. D. and Nainwal, H. C., Variation of snowline and mass balance of glaciers of Warwan and Bhut basins of western Himalaya using remote sensing technique. *J. Indian Soc. Remote Sensing*, 2011, **40**(4), 629–637.
36. Mir, R. A., Jain, S. K., Saraf, A. K. and Goswami, A., Detection of changes in glacier mass balance using satellite and meteorological data in Tirunghhad basin located in western Himalaya. *J. Indian Soc. Remote Sensing*, 2013, **42**(1), 91–105.
37. Wagnon, P. *et al.*, Four years of mass balance on Chhota Shigri Glacier, Himachal Pradesh, India, a new benchmark glacier in the western Himalaya. *J. Glaciol.*, 2007, **53**(183), 603–611.
38. RGI Consortium, Randolph Glacier Inventory – a dataset of global glacier outlines: Version 6.0. Technical Report, Global Land Ice Measurements from Space, Colorado, USA, 2017.
39. Chander, G., Markham, B. L. and Helder, D. L., Summary content radiometric calibration coefficients for Landsat MSS, TM, ETM+ and EO-1 ALI sensors. *Remote Sensing Environ.*, 2009, **113**, 893–903.
40. Kuhn, M., The response of the equilibrium line altitude to climatic fluctuations: theory and observations. In *Glacier Fluctuations and Climatic Change* (ed. Oerlemans, J.), Kluwer Academic, Dordrecht, The Netherlands, 1989, pp. 407–417.
41. Singh, V., Singh, P. and Haritashya, U., *Encyclopedia of Snow, Ice and Glaciers*, Springer Science and Business Media, Dordrecht, The Netherlands, 2011.
42. Pratap, B., Dobhal, D. P., Bhambri, R., Mehta, M. and Tewari, V. C., Four decades of glacier mass balance observations in the Indian Himalaya. *Reg. Environ. Change*, 2016, **16**, 643–653.
43. Angchuk, T., Ramanathan, A. L., Mandal, A., Soheb, M., Bahuguna, I. M., Singh, V. and Linda, A., *In situ* mass balance measurements and morphology study of Patsio Glacier, Himachal Pradesh, Western Himalaya. AGU Fall Meeting Abstracts, 2016, C11C-0797.
44. Gaddam, V. K., Kulkarni, A. V. and Gupta, A. K., Reconstruction of specific mass balance for glaciers in Western Himalaya using seasonal sensitivity characteristic(s). *J. Earth Syst. Sci.*, 2017, **126**(4), 55.
45. WGMS, Latest glacier mass balance data. World Glacier Monitoring Service, Zurich, Switzerland, 2019; <https://wgms.ch/latest-glacier-mass-balance-data/>
46. Raina, V. K., Kaul, M. K. and Sing, S., Mass balance studies of Gara Glacier. *J. Glaciol.*, 1977, **18**(80), 415–423.
47. Sangewar, C. V. and Siddiqui, M. A., Thematic compilation of mass balance data on glaciers of Satluj catchment in Himachal Himalaya. *Rec. Geol. Surv., India*, 2006, **141**(8), 159–161.
48. Srivastava, D., Glaciology of Indian Himalayas: a bilingual contribution in 150 years of Geological Survey of India. *Geol. Surv. India Spec. Publ.*, 2001, **63**, 213.
49. Singh, R. K. and Sangewar, C. V., Mass balance variation and its impact on glacier flow movement at Shaune Garang Glacier, Kinnaur, Himachal Pradesh. In Proceedings of the National Meet on Himalayan Glaciology, Department of Science and Technology, New Delhi, 1989, pp. 149–152.
50. Geological Survey of India, GSI Annual Report 1991–1992, 1992, pp. 175–176.
51. Kaul, M. K., Mass balance of Liddar glaciers. *Trans. Inst. Indian Geogr.*, 1986, **8**(2), 95–112.
52. Koul, M. N. and Ganjoo, R. K., Impact of inter- and intra-annual variation in weather parameters on mass balance and equilibrium line altitude of Naradu Glacier (Himachal Pradesh), NW Himalaya, India. *Climatic Change*, 2010, **99**(1), 119–139.
53. Ramanathan, A. L., Status report on Chhota Shigri Glacier (Himachal Pradesh), Himalayan Glaciology Technical Report No. 1, Department of Science and Technology, New Delhi, 2011, p. 88.
54. Mishra, R., Kumar, A. and Singh, D., Long term monitoring of mass balance of Hamtah Glacier, Lahaul and Spiti district, Himachal Pradesh. *J. Geol. Surv. India*, 2014, **147**, 230–231.
55. Bhutiyan, M. R., Mass-balance studies on Siachen Glacier in the Nubra Valley, Karakoram Himalaya, India. *J. Glaciol.*, 1999, **45**(149), 112–118.

ACKNOWLEDGEMENTS. We thank the ESSO-National Centre for Antarctic and Ocean Research (Ministry of Earth Sciences, Government of India), Goa for providing financial support under the HiCOM (Sanction Order No: NCAOR/2018/HiCOM/06, 28 March 2018) initiative to undertake this research. We also thank Dr Krishna Venkatesh (Director, CIIRC-Jyothy Institute of Technology, Bengaluru) and Sri Sringeri Sharada Peetham, Sringeri, for help and support.

Received 5 March 2020; revised accepted 21 September 2020

doi: 10.18520/cs/v119/i12/1961-1973